NANO · MICRO small

www.small-journal.com

# The Role of Temperature and Lipid Charge on Intake/Uptake of Cationic Gold Nanoparticles into Lipid Bilayers

*Fabio Lolicato, Loic Joly, Hector Martinez-Seara, Giovanna Fragneto, Ernesto Scoppola, Francesca Baldelli Bombelli, Ilpo Vattulainen, Jaakko Akola,* and Marco Maccarini**

**Understanding the molecular mechanisms governing nanoparticle–membrane interactions is of prime importance for drug delivery and biomedical applications. Neutron reflectometry (NR) experiments are combined with atomistic and coarse-grained molecular dynamics (MD) simulations to study the interaction between cationic gold nanoparticles (AuNPs) and model lipid membranes composed of a mixture of zwitterionic di-stearoyl-phosphatidylcholine (DSPC) and anionic di-stearoyl-phosphatidylglycerol (DSPG). MD simulations show that the interaction between AuNPs and a pure DSPC lipid bilayer is modulated by a free energy barrier. This can be overcome by increasing temperature, which promotes an irreversible AuNP incorporation into the lipid bilayer. NR experiments confirm the encapsulation of the AuNPs within the lipid bilayer at temperatures around 55 °C. In contrast, the AuNP adsorption is weak and impaired by heating for a DSPC–DSPG (3:1) lipid bilayer. These results demonstrate that both the lipid charge and the temperature play pivotal roles in AuNP–membrane interactions. Furthermore, NR experiments indicate that the (negative) DSPG lipids are associated with lipid extraction upon AuNP adsorption, which is confirmed by coarse-grained MD simulations as a lipid-crawling effect driving further AuNP aggregation. Overall, the obtained detailed molecular view of the interaction mechanisms sheds light on AuNP incorporation and membrane destabilization.**

## 1. Introduction

The enhanced use of nanoengineered materials exposes humans, animals, and the environment to their potential risks.[1] Therefore, it is imperative to gain fundamental understanding of the undesired effects of nanoparticles on living systems that go beyond their primary function. The toxicity of nanoparticles and, more generally, their interaction with plasma membranes depends in a complex manner on several factors such as the size,[2] shape,[3,4] charge,[5,6] concentration, and functionalization of the nanoparticle.[7] The complexity of nanotoxicity studies is further increased by the fact that in vitro observations of toxicity are often not representative nor directly transferable to in vivo studies.[8]

Since the first contact between a nanoparticle and a living cell occurs through a biological membrane, it is important to understand the basic mechanisms governing the interaction with the plasma membrane. However, real membranes

F. Lolicato, Prof. I. Vattulainen, Prof. J. Akola
Computational Physics Laboratory
Tampere University
P.O. Box 692, FI-33014 Tampere, Finland

F. Lolicato, Prof. I. Vattulainen
Department of Physics
University of Helsinki
P.O. Box 64, FI-00014 Helsinki, Finland

L. Joly, Prof. F. Baldelli Bombelli
Laboratory of Supramolecular and BioNano Materials
Department of Chemistry, Materials and Chemical Engineering
Politecnico di Milano
via Mancinelli 7, 20131 Milano, Italy

The ORCID identification number(s) for the author(s) of this article can be found under https://doi.org/10.1002/smll.201805046.



**DOI: 10.1002/smll.201805046**

L. Joly, Dr. G. Fragneto
Institut Laue-Langevin
71 Avenue des Martyrs, 38042 Grenoble, France

Dr. H. Martinez-Seara
Institute of Organic Chemistry and Biochemistry
of the Czech Academy of Sciences
Flemingovo nám. 2, 16610 Prague 6, Czech Republic

Dr. E. Scoppola
Max Planck Institute of Colloids and Interfaces
14476 Potsdam, Germany

Prof. I. Vattulainen
MEMPHYS–Center for Biomembrane Physics

Prof. J. Akola
Department of Physics
Norwegian University of Science and Technology
NO-7491, Trondheim, Norway
E-mail: jaakko.akola@ntnu.no

Dr. M. Maccarini
Laboratoire TIMC-IMAG
Université Grenoble Alpes
Domaine de la Merci, 38706 La Tronche Cedex, France
E-mail: marco.maccarini@univ-grenoble-alpes.fr

 

are complex in terms of their structure, composition, and properties (e.g., presence of several lipid types, cholesterol, membrane proteins, glycocalyx), and hence it is currently difficult to establish models that can predict the fate of nanoparticles interacting with a real plasma membrane nor to estimate the effect of the interaction on the membrane structure and stability. Instead, simpler models can be used to represent some essential membrane characteristics. At the same time, they can be produced in a controlled and reproducible way to allow a precise characterization with a range of experimental techniques. Ultimately, model membranes enable to quantify and decouple the effects of different factors that determine the interaction of nanoparticles with lipid bilayers.[9–11] The possibility to tune lipid composition enables systematic studies on how individual lipids affect the nanoparticle interaction, and this is instrumental for the present article.

To shed light on the nanoparticle–membrane interaction, we utilize here gold nanoparticles (AuNPs) that have generated a wide interest in the field of nanotechnology due to their intriguing properties, such as the size-dependent stability, ligand-protection, quantum size effects, and single-electron transitions.[12–14] The smallest AuNPs of sizes below ≈2 nm core diameter and including up to a few hundred Au atoms exhibit characteristic electronic effects based on simple quantum-mechanical rules of the superatomic electronic structure.[15] Together with geometrical shell closings (e.g., icosahedra, decahedra) and possible ligand-protection, this causes that the physicochemical properties of AuNPs have a strong dependence on their size and shape.[16] AuNPs are used in a broad spectrum of applications such as molecular recognition[17,18] and specific binding to biomolecules[19–22] with significant implications for biological and biomedical studies.[23,24] The corresponding AuNPs are typically ligand-protected where the surrounding side groups can be varied, and they are mainly responsible for the interaction with membranes.

Even for simpler model systems, the study of the interaction between AuNP and lipid membranes still presents major difficulties in view of the high number of parameters involved. Theoretically, the details of the AuNP–membrane interaction are of great interest and there have been several molecular dynamics (MD) investigations.[25–35] Of particular interest has been the effect of the AuNP charge (as determined by the ligand terminal groups) and the lipid bilayer composition which determine the nanoscale details of the attachment (or its absence). For example, all-atom MD simulations have shown for zwitter-ionic lipids that a cationic AuNP induces disruption of the lipid head-group arrangement exposing the hydrophobic region of the membrane to the nanoparticle.[26] The opening of the small circular patch in the lipid headgroup region can be considered as the onset of the penetration process. It has also been reported that AuNPs with amphiphilic side chains can penetrate in defect-free low-curvature membranes due to the hydrophobic interplay between the AuNP side chains and lipids.[28] The transmembrane state is stabilized by "snorkeling" or "anchoring" where the charged AuNP terminal groups reach out of the bilayer interior.[31,36]

Experimentally, nanostructural studies performed with neutron reflectometry (NR) have focused on the mediating effect of the protein corona on the interaction between 20 and 100 nm diameter carboxylated polystyrene nanoparticles and solid supported lipid bilayer (SLB),[37] and on the effect of the lipid composition on the interaction between 10 nm super paramagnetic iron oxide nanoparticles and SLB.[38] However, the strong interaction between the bilayer and the supporting substrate can have an unpredictable impact on the membrane properties. Among different types of model membranes, floating lipid bilayers are formed by placing a lipid bilayer floating at a nanometer distance above an SLB.[39,40] Floating bilayers have the advantage of being highly hydrated and fluctuating with dynamical properties comparable to those of biological membranes. We have previously shown with NR studies[6] that this choice provides a membrane system which is sufficiently stable to withstand the interaction with AuNP while retaining high enough sensitivity to show significant nanostructural changes.

Here, we present a combined neutron scattering and MD simulation approach to clarify some key aspects of the interaction mechanism between cationic AuNPs and lipid bilayers at the atomistic scale. The study focuses on the effects of two external parameters, temperature and concentration of negatively charged lipids. The lipid charge is highly relevant for biological systems as plasma membranes are negatively charged, whereas the temperature can be used here to tune the system across the gel transition (phase of the lipid bilayer). We show how the presence of charged lipids determines the fate of AuNP (adsorption or internalization) and how the AuNP–interaction responds to temperature in the case of noncharged and negatively charged bilayers. Moreover, we show also by coarse-grained MD how the lipid charge affects the cooperative behavior of AuNPs (aggregation) which can turn out fatal for the membrane stability.

## 2. Results

### 2.1. Neutron Reflectivity Measurements

The effect of cationic $Me_3N^+$AuNPs on the nanoscale organization of the lipid bilayers was studied by NR with three different lipid compositions: pure 1,2-distearoyl-*sn*-glycero-3-phosphocholine (DSPC) (Sample 1); dDSPC/1,2-distearoyl-*sn*-glycero-3-phospho-(1′-*rac*-glycerol) (sodium salt) (DSPG) (3:1) (Sample 2); and DSPC/DSPG (9:1) (Sample 3). The measurements were made at different solvent deuteration grades. Using different isotopic compositions of the solvent changed the reflectivity profile while largely preserving the same chemical structure (contrast variation). Details of the used contrast are given in the Experimental Section.

#### *2.1.1. Pure DSPC Bilayer Floating on a Supported Bilayer*

The pure DSPC bilayer system was prepared by Langmuir–Blodgett and Langmuir–Schaefer techniques and measured in three contrasts as described in ref. [6]. The data were analyzed using the new Fit Model I (see the Experimental Section), which accounts for possible macroscopic regions of the Si substrate surface that are free from the floating bilayer.

**Figure 1**A shows the reflectivity profiles of the pure DSPC bilayer system, and the curves used to fit the data. Figure 1B depicts the corresponding scattering length density (SLD) profiles complemented by a visual illustration of the systems. The structural parameters obtained from the fitting analysis

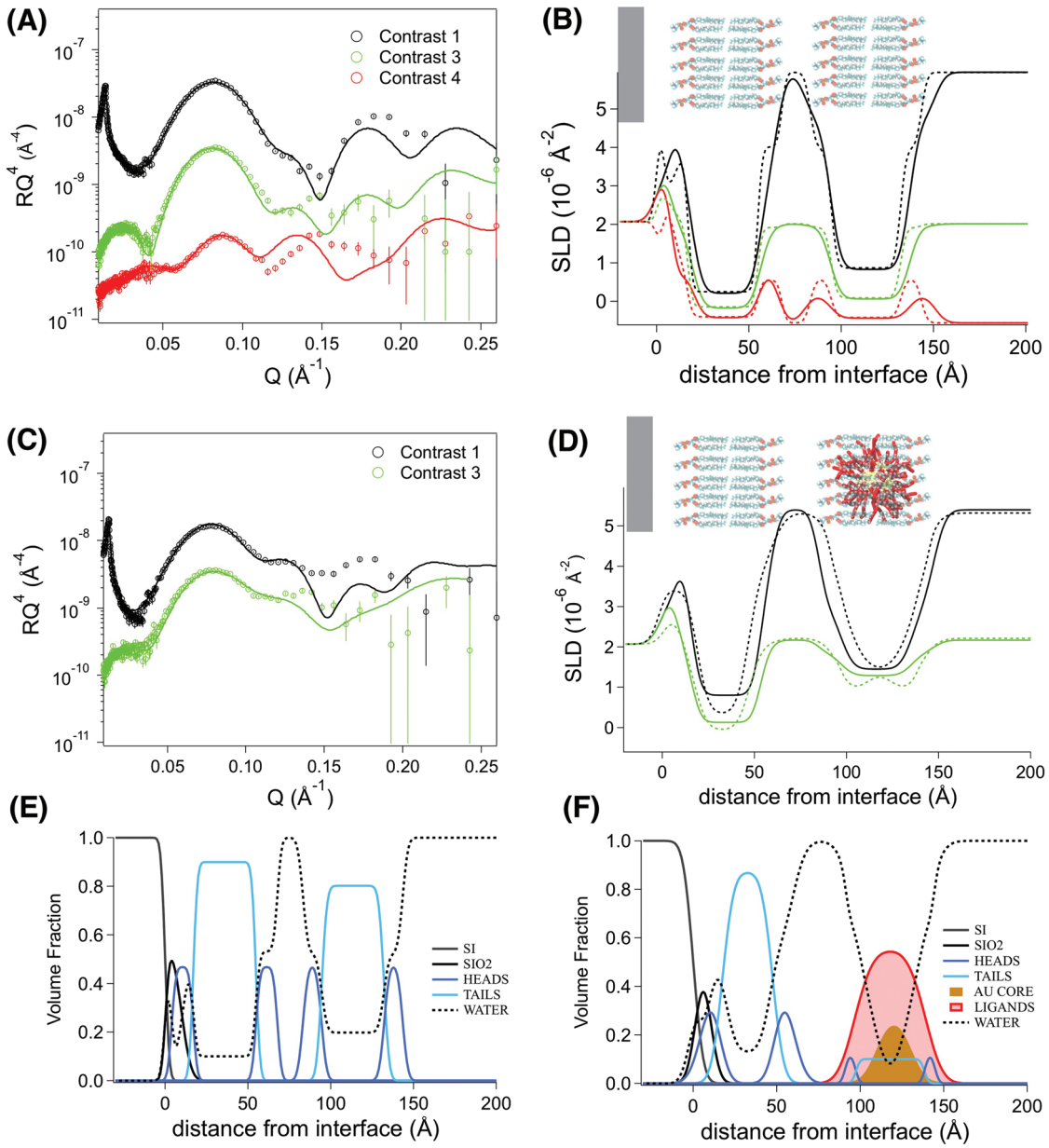


**Figure 1.** A) Reflectivity profiles of the pure DSPC bilayer system measured at different contrasts (symbols), and the corresponding fits (lines). B) SLD profile corresponding to the fits in (A) obtained with Fit Method 1 (solid lines) and those obtained with Fit Method II (dashed lines), and a schematic view of the lipid system. C) Reflectivity profiles of the floating DSPC bilayer measured at different contrasts after the exposure to cationic $Me_3N^+$AuNPs (symbols), and the corresponding fits (lines). D) SLD profile corresponding to the fits in (C) and a schematic view of the lipid–AuNP system. E) Volume occupancy profile of the molecular components present in the pristine membrane system, and F) after the interaction with the AuNP. All measurements refer to Sample 1 and were performed at 25 °C. Between the measurements shown in (A) and (B), (C) and (D), and (E) and (F) the system underwent an annealing process at 53 °C The reflectivity curves have been off-set vertically for clarity.

(Table S1, Supporting Information) are consistent with previously published results.[6] After exposure to an aqueous solution containing cationic $Me_3N^+$AuNPs (0.01 mg $mL^{-1}$), no significant changes in the reflectivity profile were observed,[6] if the exposure was carried out at 25 °C. However, changes in reflectivity were obvious, when the temperature was raised to 53 °C and then lowered back to 25 °C. The reason for increasing the temperature to 53 °C, which is still below the gel-fluid phase transition of DSPC (55 °C) is that lifting the temperature above the gel-fluid phase transition in the presence of cationic AuNPs leads to destabilization of the floating bilayer.[6] The effect of temperature on the properties of the floating lipid bilayer system was already addressed in previous studies.[39,40]

At 25 °C, after the temperature quench, further flowing of water in the liquid subphase did not alter the reflectivity profile. The structural configuration of the AuNP-lipid system remained stable. Figure 1C–D shows the reflectivity profiles, the best fits, and the corresponding SLD profiles, and Table S1 (Supporting

Information) lists the resulting structural parameters. By comparing the parameters of the pure DSPC bilayer system with those found after the exposure to AuNPs (Table S1, Supporting Information), we noticed that the interaction with the AuNPs gave rise to considerable changes: the SLD of the tail region (not including the aqueous components) of the floating bilayer increased significantly ($1.2 \times 10^{-6}$ vs $-0.41 \times 10^{-6}$ Å$^{-2}$), and the hydration of the floating lipid bilayer decreased substantially (from ≈20% to ≈5%). The latter is confirmed by the values of the parameters in Table S1 (Supporting Information) and from the vertical distance of the two SLD profiles in the tail region in Figure 1B compared to Figure 1D. The higher the hydration of the region, this distance becomes more pronounced. This is consistent with the incorporation of AuNPs (SLD of the Au core being $4.5 \times 10^{-6}$ Å$^{-2}$) into the floating bilayer with consequent displacements of water molecules. Furthermore, the interstitial layer between the floating and the supporting bilayer was thicker, and there was a change in hydration in the supported lipid bilayer.

These results were confirmed by performing the analysis of the reflectivity profiles with the Fit Method II described in the Supporting Information. The difference between the two fitting methods arises from the SLD profile construction. In Fit Method I, the SLD profile was divided in slabs whose parameters (thickness, SLD, water content, roughness) were determined by fitting the model reflectivity profile to the reflectivity data. In Fit Method II, the volume fraction distribution of the molecular species, which depends on the relative amount of each species and their relative positions, was first generated. Subsequently, the SLD profile corresponding to this distribution and the reflectivity profiles were calculated. The volume fraction distribution was then optimized by comparing the resulting reflectivity profiles with the experimental data. The method was initially tested for consistency on the pristine bilayer (Figure 1B) giving comparable results. The two methods give in general comparable results in terms of SLD (see Figure 1D). Moreover, Fit Method II returns directly the volume occupancy of all species present across the interface (Figure 1E–F) and the area per AuNP in the floating lipid bilayer ($500 \pm 20$ Å$^2$ molecule$^{-1}$).

Next, the lipid bilayer system was exposed to a 0.01 mg mL$^{-1}$ solution of cationic $Me_3N^+$AuNPs, incubated for 30 min at 25 °C, and then flushed with pure solvent at three contrasts. The reflectivity profiles are shown in Figure 2C along with the best fits to the data. The resulting SLD profiles are shown in Figure 2D. To fit the reflectivity curves, it was necessary to include an additional hydrated layer on top of the floating bilayer having a thickness and SLD comparable to those of AuNP. This suggests that some AuNPs adsorbed on the outer surface of the floating bilayer. A model without this extra layer of AuNP resulted in a weaker representation of the reflectivity data with a 40% increment of the $\chi^2$ (see Figure S1 in the Supporting Information). By comparing Figure 2B,D, we find also that the SLD of the floating bilayer becomes asymmetric. This effect could be due to AuNP adsorption to the outer leaflet, therefore inducing changes to the solvent distribution across the floating bilayer (see Table S2 in the Supporting Information).

The sample was then annealed at 65 °C, gradually cooled down to 25 °C, and consecutively characterized in four contrasts (Figure 2E–F and Table S2, Supporting Information). As shown in Figure S2 (Supporting Information), the reflectivity profiles were significantly affected by AuNPs at 25 °C. However, after annealing the reflectivity profiles changed back to their low-temperature behavior in a manner that is very similar to that observed in the pure bilayer system, with an exception concerning the region around the first minimum at $Q \approx 0.025$ Å$^{-1}$. The analysis confirmed that the annealed lipid bilayer had structural parameters similar to those of the pure system, with a slightly reduced coverage that affected mainly the region of the first minimum in the reflectivity profile. The overall picture of increased roughness in the floating bilayer makes it difficult to unequivocally resolve the precise details, but the model best fitting the data suggests that the annealing caused AuNPs desorption from the bilayer surface, and that AuNP desorption caused some lipids (including both DSPC and DSPG) to be extracted from the bilayer.

#### 2.1.2. dDSPC/DSPG (3:1) Bilayer Floating on a Supported Bilayer

The reflectivity profiles for the dDSPC bilayer system containing 25 mol% negatively charged DSPG were measured at 25 °C using four different contrasts. In this case, we opted for a fully deuterated dDSPC and a hydrogenous DSPG. This isotopic difference allows to decouple the structural contribution of the two components. **Figure 2**A–B shows the reflectivity profiles, the fits, and the corresponding SLD profiles. The structural parameters obtained by the fitting analysis are listed in Table S2 (Supporting Information). Interestingly, we find that the SLDs of the inner and outer leaflets of the supported bilayer are significantly different. This suggests the transmembrane distributions of dDSPC and DSPG to be asymmetric, probably due to the electrostatic interaction between the negatively charged DSPG and the negative charges present on the surface of the Si substrate. Given that the SLD of the deuterated tail of DSPC is $7.07 \times 10^{-6}$ Å$^{-2}$ and that of the hydrogenous tail of DSPG being $-0.41 \times 10^{-6}$ Å$^{-2}$, we estimated the dSDPC/DSPG ratio in the inner and outer leaflet of the supported bilayer to be 8:2 and 7:3, respectively. This asymmetry in the lipid distribution was not observed in the floating bilayer leaflets, where the SLDs were similar.

#### 2.1.3. DSPC/DSPG (9:1) Bilayer Floating on a Supported Bilayer

The reflectivity profiles of the lipid bilayer having an intermediate DSPG lipid content (10 mol%), was measured at 25 °C with three water contrasts. **Figure 3**A–B shows the measured reflectivity profiles, the best fits, and the corresponding SLD profiles. The corresponding structural parameters are listed in Table S3 (Supporting Information).

Successively, the lipid bilayer system was exposed to a 0.01 mg mL$^{-1}$ solution of cationic $Me_3N^+$AuNPs and incubated for 30 min at 25 °C. The reflectivity profiles did not show significant changes at this point. Some significant changes occurred only after the sample was annealed at 65 °C and then gradually brought back to 25 °C. After rinsing with pure solvent, the sample was characterized with different contrasts. The resulting reflectivity profiles are shown in Figure 3C along with the best fits to the data. The model used to fit the data encompassed a well-defined supported bilayer above which two leaflets floated, having different thicknesses, SLDs, water content, and a significantly higher

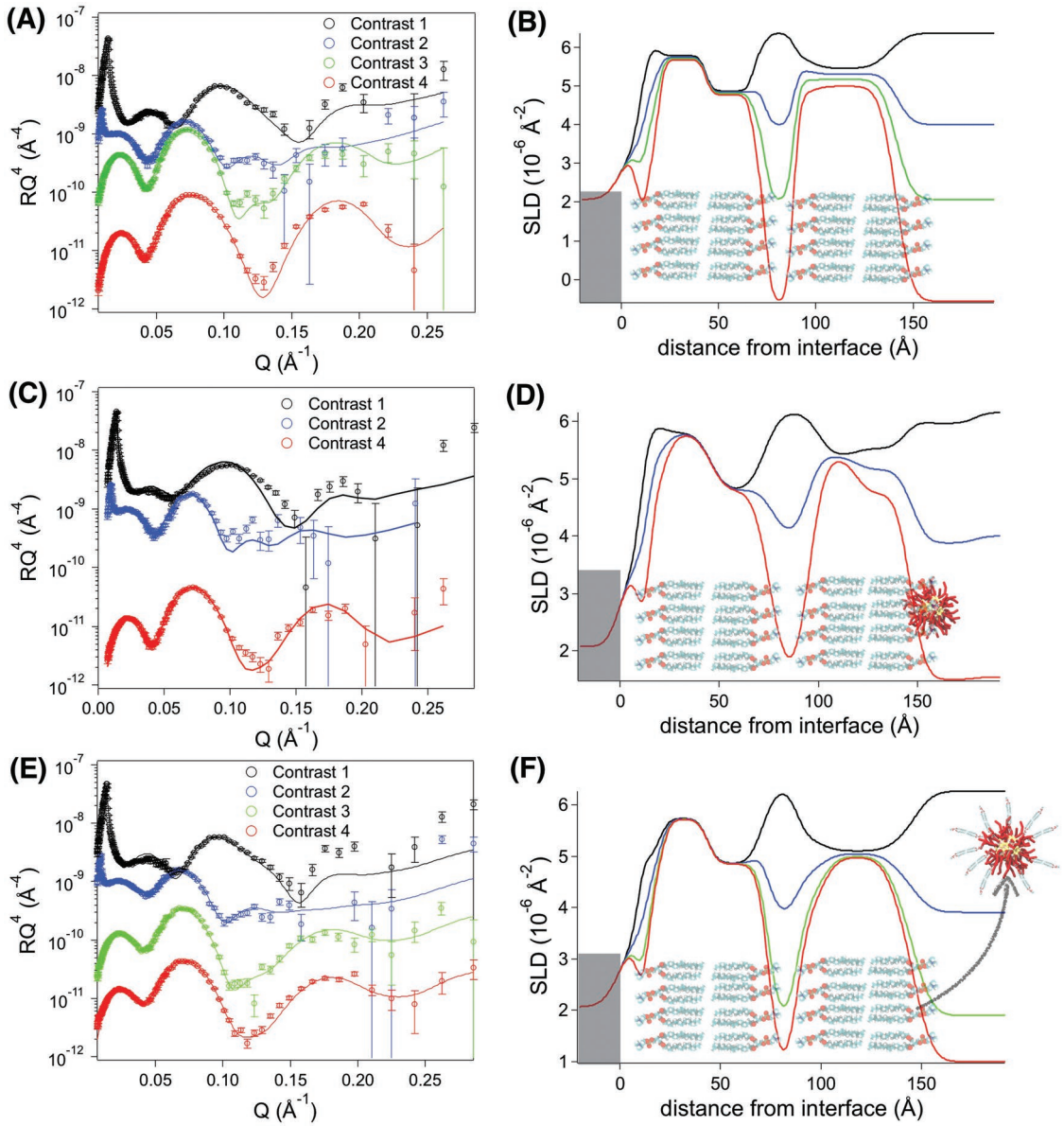


**Figure 2.** A) Reflectivity profiles of the pristine dDSPC/DSPG (3:1) lipid bilayer measured at different contrasts (symbols) and fits (lines) at 25 °C. B) SLD profile corresponding to the fits in (A) and a schematic view of the lipid system. C) Reflectivity profiles of the dDSPC/DSPG (3:1) lipid bilayers measured at different contrasts (symbols) after the exposure to the cationic $Me_3N^+$AuNPs at 25 °C, including fits (lines). D) SLD profile corresponding to the fits in (C) and a schematic view of the lipid-AuNP system. E) Reflectivity profiles of the dDSPC/DSPG (3:1) lipid bilayers measured at different contrasts (symbols) after the exposure to the cationic $Me_3N^+$AuNPs and annealing at 65 °C, including fits. For clarity, the reflectivity curves are off-set vertically.

roughness. This suggests that the presence of AuNPs altered significantly the ordered structure of the floating lipid bilayer, which resulted in smeared out and consequently less defined SLDs. The higher SLD on the outer leaflet suggests a more pronounced presence of AuNPs in this layer, rather than in the inner leaflet (Table S3, Supporting Information). This indicates a combined effect of partial or total inclusion of AuNPs in the floating bilayer, adsorption of AuNPs in the floating bilayer, and extraction of lipids by the nanoparticles.

To better resolve the SLD profile linked to the reflectivity curves, we applied the Fit Method II described in the Supporting information. Also in this case, the method was initially tested for consistency on the pristine bilayer. The model provided a good fit of the reflectivity curves (see Figure S3A in the Supporting Information). The SLD profiles obtained with the two methods shown in Figure 3B are consistent with each other. The volume fractions of each component as a function of the distance from the substrate are reported in Figure 3E. The Fit Method II was then applied to analyze the reflectivity profiles in the presence of AuNP. The fits displayed in Figure S3B show good agreement with the data. As shown in Figure 3D, also the resulting SLD profiles were consistent with those obtained with the Fit Method I. In addition, the refinement returned the results described

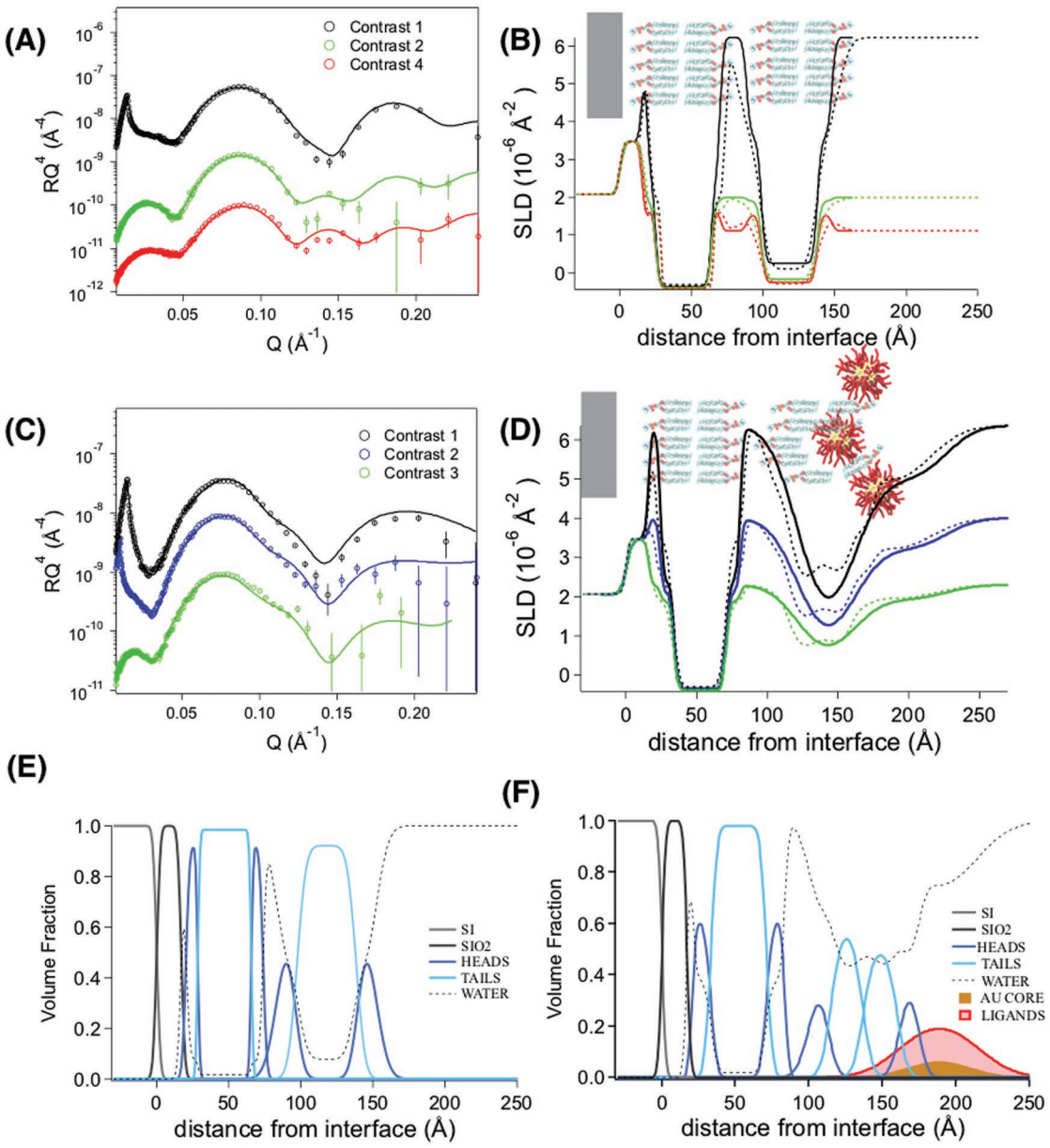


**Figure 3.** A) Reflectivity profiles of the pristine DSPC/DSPG (9:1) lipid bilayers measured at different contrasts (symbols) at 25 °C, and fits made to the data obtained with the Fit Method I (lines). B) SLD profile corresponding to the fits in (A) obtained with the Fit Method I (solid lines) and the Fit Method II (dashed lines), and a schematic view of the lipid system. C) Reflectivity profiles of the DSPC/DSPG (9:1) lipid bilayers measured at different contrasts (symbols) after the exposure to the cationic $Me_3N^+$AuNPs, and the corresponding best fits to the data (lines). The measurements were performed at 25 °C after an annealing cycle at 65 °C. D) SLD profile corresponding to the fits in (C) and a schematic view of the lipid–AuNP system. For clarity, the reflectivity curves are off-set vertically. E) Volume occupancy profile of the molecular components present in the pristine membrane system, and F) after the interaction with the AuNP.

in Figure 3E in terms of distribution of volume fractions as a function of the distance from the Si surface. The presence of a lipid bilayer supported on the Si substrate was evidenced in agreement with the previous analysis. On top of this lipid bilayer, the new analysis showed the presence of a mixed layer composed of lipid bilayers and AuNP (Figure 3F) with an area per AuNP of 610 ± 20 Å$^2$ molecule$^{-1}$. The average position of AuNPs was unbalanced toward the outer leaflet of the lipid bilayer, and the floating layer is significantly more hydrated than the pristine bilayer. The numerical values of the fits are listed in Table S5 in the Supporting Information.

### 2.2. Results of Molecular Dynamics Simulations

The AuNP-membrane system was simulated in the fluid and gel phases, i.e. at 343 and 300 K, respectively, by using atomistic (AA) and coarse-grained (CG) models, and the simulation

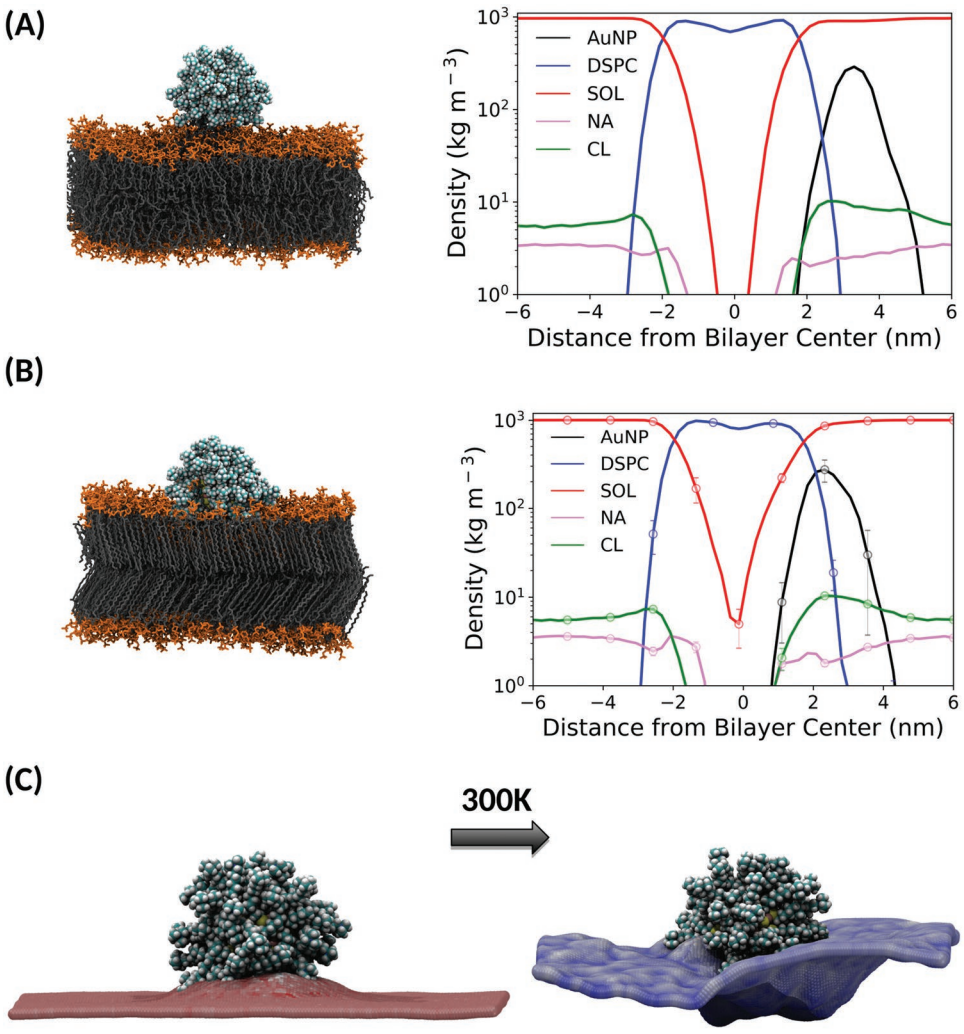


**Figure 4.** A) Left, a snapshot of AuNP interacting with the DSPC membrane surface taken from the AA simulation at 343 K after 200 ns (liquid phase). AuNP is represented with van der Waals beads of cyan color for carbon, white for hydrogen, blue for nitrogen, yellow for sulfur, and pink for gold atoms. The DSPC lipids are visualized with the licorice style; the hydrophobic chains in grey and the polar head groups in orange. Water and ions are not visible for clarity. Right, the corresponding partial density profile averaged over the last 50 ns in the same vertical distance scale. B) Left, a snapshot of AuNP interacting with the DSPC membrane surface taken after 200 ns of cooling down the simulation to 300 K (gel phase). Right, the corresponding partial density profile averaged over the last 50 ns. The standard error is calculated considering the three repeated simulations as independent samples. C) Visualization of the local membrane curvature around AuNP averaged over the last 50 ns at 343 K (left) and 300 K (right).

setups and times have been summarized in Table S7 (Supporting Information). Both atomistic and CG MD simulations indicate that the positively charged AuNP, which mimics closely the experimental one (2 nm diameter—see Figure S4 in the Supporting Information), is not able to attach to the pure DSPC membrane spontaneously. This result, which is consistent with previously published data,[26] seems to contradict our experimental findings at least in the liquid-disordered phase (343 K). However, the same data demonstrate the existence of a substantial but not prohibiting energy barrier for the approach of AuNP toward the membrane surface. Still, the time scale for the event to occur spontaneously in an unbiased simulation is beyond current simulation time scales. Upon forcing the AuNP, to approach the membrane surface, it results in the formation of a stable contact as shown in **Figure 4**, where the negatively charged phosphate atoms of DSPC and the positively charged choline groups of the 11-mercaptoundecantrimethylammonium chains of AuNP interact in a favorable manner. The phosphate region of the DSPC bilayer reorganizes beneath AuNP by tilting the phosphate groups and AuNP side chains away from the contact region (Figure S5, Supporting Information). This results in a circular patch opening in the membrane surface which now exposes its hydrophobic region to AuNP. We consider this process as the first step toward AuNP penetration, as was described first in ref. [26].

The nanoparticle attached to the DSPC membrane is simulated for 200 ns at 343 and 300 K with the AA force field, and the corresponding visualizations and partial density profiles are shown in Figure 4A,B. At both temperatures, the AuNP remains attached to the surface and the circular patch does not open further even when the membrane becomes more corrugated (gel-phase). The membrane is in a fluid phase at

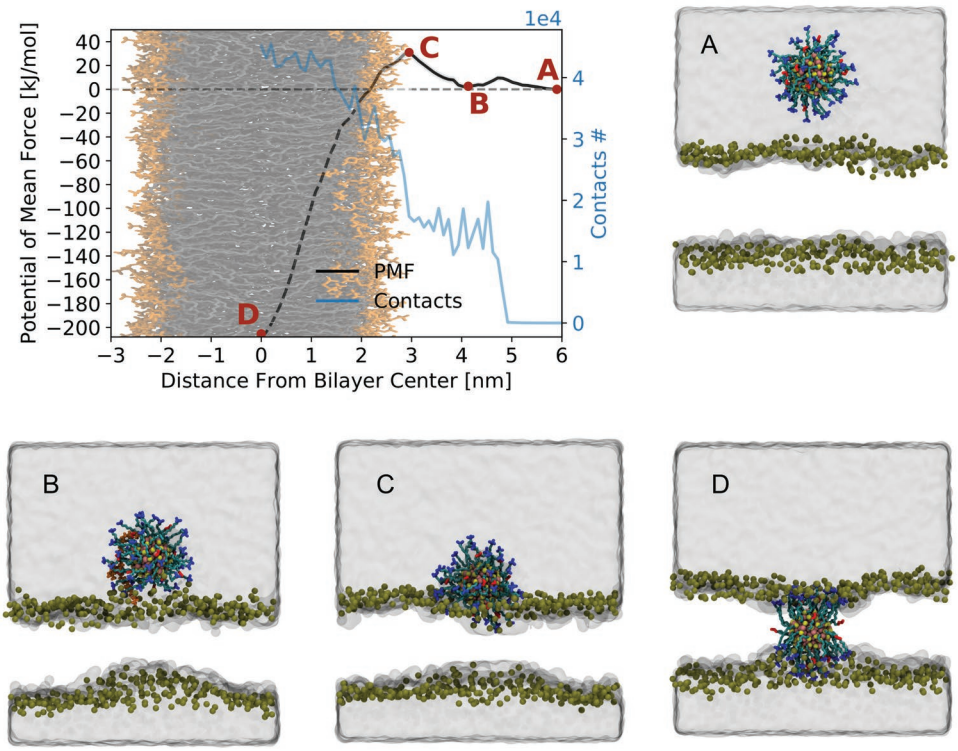


**Figure 5.** AuNP intake described by the free energy profile, and visualizations of the four key steps of the insertion pathway. A) The equilibrium position in the water phase. B) The first free energy minimum on the bilayer surface after opening a small circular patch at the membrane surface (a free energy barrier of 10 kJ mol$^{-1}$). C) Free energy maximum at 32 kJ mol$^{-1}$ with a partial insertion of the AuNP in the upper leaflet of the membrane. D) The position inside a membrane with the AuNP chains rearranged to expose the polar head groups to water on both sides of the bilayer. The black line shows the PMF profile, whereas the blue line depicts the number of contacts (within a distance <6 Å) between any pair of atoms between AuNP and the bilayer along the reaction coordinate. The dashed line describes the region where a more advanced reaction coordinate would likely be useful in order to fully sample the anchoring of charged ligands to the distal leaflet. Water is represented by a translucent surface whereas DSPC phosphates are shown as van der Waals (VdW) spheres. The AuNP core is represented with pink (gold) and yellow (sulfur) VdW -spheres and the side chains are shown in licorice style with cyan color. The terminal trimethylammonium groups are colored in blue and octanethiol groups in red.

343 K. Surface curvature analysis using the coordinates of the phosphorus atoms at the contact point shows that AuNP is sitting on a positive curvature region that results in the above mentioned lipid head group reorganization (Figure 4C, left). Inducing the transition to the gel phase by lowering the temperature leads to a significant corrugation of the membrane surface (Figure 4C, right); however, the reorganized phosphate head group network remains unchanged, as shown in Figure S5 (Supporting Information). This membrane corrugation is clearly seen in the corresponding water and counter-ion density profiles obtained as the average over three independent replicas of the gelification process (Figure 4B). AuNP appears to be immersed deeper in the gel phase (300 K, Figure 4B–C), but this behavior can be mostly explained by the preferential location of the AuNP in the formed valleys (local negative curvature).

Our atomistic and coarse-grained MD simulations reveal that AuNP is not able to attach to the DSPC membrane spontaneously neither at 343 K nor at 300 K. This is expected based on the experiments at 300 K, yet the higher temperature highlights a problem with the finite time-scale of the AA simulations. To improve sampling and calculate the free energy required to bring AuNP in contact with the membrane at 343 K, we employed the umbrella sampling technique.[41] Besides promoting the contact between AuNP and membrane, this method also evaluates the free energy profile of the membrane insertion process (**Figure 5**). The pathway through the points **A–D** along the free energy profile is explained as follows.

We shift the energy profile such that the point **A**, when the AuNP still does not feel the presence of the membrane, corresponds to 0 kJ mol$^{-1}$. After a local minimum at **B**, we see a sizable free energy barrier for the primary stage of the AuNP insertion of 32.4 kJ mol$^{-1}$ at **C** after which the process of introducing a AuNP into the membrane is very favorable, demonstrated by a free energy fall until −208 kJ mol$^{-1}$ at **D**. As indicated in Figure 4 for unbiased simulations, the insertion process shows a metastable minimum at point **B**, where AuNP is in contact with the membrane surface. It corresponds to a distance around 4.0 nm between the AuNP center of mass and the bilayer center (free energy 2.5 kJ mol$^{-1}$). The approaching nanoparticle has to overcome a small free energy barrier of ≈10 kJ mol$^{-1}$ to adjust the choline arrangement of DSPC, while stabilizing the electrostatic interactions between the trimethylammonium groups (AuNP) tails and phosphates. These changes of lipid orientations within the upper leaflet are reflected also in the lower leaflet and show up as a negative curvature of the membrane bottom surface. The simulations demonstrate also lipid extraction, as shown in Figure 5B, where the lipid crawling

on AuNP has been colored orange. This lipid extraction starts with the contact between the AuNP chains and a lipid tail protrusion facing the water layer (see Video S1 in the Supporting Information). The interaction with the solvent-accessible lipid tail is a key step of the permeation process, driving the insertion into the upper leaflet as Van Lehn et al. have shown.[42]

Previously, a similar free energy barrier for an approaching AuNP was found at the same distance with respect to the center of mass of the membrane.[26] However, the local minimum at the membrane surface was more stable with a negative free energy value (–18.3 kJ $mol^{-1}$). This mismatch can be assigned to differences in the AuNP side groups as the corresponding nanoparticle model structure was 25% more charged with 60 terminal ammonium groups. Furthermore, the smaller ammonium groups can penetrate deeper within the phosphate region and establish several hydrogen bonds each with the lipids, while such bonds are absent for the choline groups.

Further insertion of AuNP from **B** inward results in a significant increase in free energy until the maximum at point **C**. During this phase, the AuNP tails have to stretch and bend while pulling apart the lipids below the AuNP core, and the hydrophilic (shorter) side chains enter the inner part of the bilayer. This is costly (32.4 kJ $mol^{-1}$), but the free energy barrier is most probably overestimated due to the difference in surface tension between the two leaflets owing to the presence of AuNP and periodic boundary conditions in the lateral direction.

After **C**, the free energy profile reduces drastically until the minimum value of –208 kJ $mol^{-1}$ is reached at **D**. This corresponds to a stable configuration where AuNP is situated symmetrically in the middle of the membrane with its charge side chains divided between the two leaflets. The octanethiol chains are aligned within the hydrophobic center region of the DSPC bilayer, while the polar and charged (longer) trimethylammonium groups extend toward the water phase on both interfaces along with the lipid head groups. This configuration is further stabilized by the hydrophobic interaction between the lipid tails and AuNP side chains. Finally, we remark that the limiting step of the AuNP-membrane interaction, in the transition from the configurations **C** and **D**, is the translocation of the charged groups of the AuNP ligands across the bilayer, as shown by Salassi et al.[43] However, due to the chosen reaction coordinate which drives the AuNP center-of-mass instead of individual side groups, we were not able to observe the iterative "flip" across the bilayer recently predicted by van Lehn and Alexander-Katz.[44] Due to the complexity of the free energy landscape and the length of the path for describing the AuNP–membrane encapsulation, using the same reaction coordinate for the whole process is a limiting factor. This specific step of the AuNP internalization process has been investigated with a better tailored reaction coordinate.[33,43,44] Their results suggest that several energy barriers between **C** and **B** associated with side chain anchoring, which are absent in our PMF, depend on the reaction coordinate chosen due to the time limitations.

**Figure 6** shows AuNP in contact with the DSPC/DSPG (3:1) membrane at 343 and 300 K. The nanoparticle interacts strongly with the membrane in the presence of 25 mol% of DSPG lipids for both the AA and CG simulations. Here, the negatively charged DSPG lipids remove the barrier observed for pure DSPC systems, promoting the cationic AuNP binding on the bilayer surface. Moreover, the partial density profiles in the liquid phase (343 K) (Figure 6A) of both lipid types show a stronger overlap with AuNP than for the pure DSPC bilayer. For this mixture in the liquid phase, the membrane surface has a smaller but existing negative curvature (Figure S7B, Supporting Information). However, a new important interaction arises between the positively charged choline terminal groups of AuNP and the DSPG phosphates. This results in the accumulation of the DSPG lipids around the nanoparticle. As before, cooling down to 300 K (gel phase) corrugates the membrane. The deeper insertion of the nanoparticle (Figure S7C, Supporting Information) is mostly explained by the more accentuated corrugation of the membrane, not self-penetration, due to the 2-component mixture and local concentration fluctuations.

It is important to emphasize that the time scale of AA simulations is limited to a few hundred nanoseconds. To investigate the system dynamics in a prolonged time scale at 343 K, we have carried out CG simulations for the same system. The results after 21 μs are visualized in Figure 6C–D. The most relevant findings are i) There are lipids crawling on the AuNP surface. These comprise both DSPC and DSPG, in agreement with the reduced lipid coverage observed experimentally (Table S2, Supporting Information). ii) The long AuNP side chains with choline terminal groups interact with DSPG and DSPC of the lower leaflet causing a local stress to the lower leaflet (Figure 6C). iii) The presence of the nanoparticle alters the local lipid concentration of the membrane, as is shown in the partial density analysis (Figure 6D), where the negatively charged DSPG accumulates around the nanoparticle. Together these results give the first indication that the presence of AuNPs may have considerable effects in the DSPC/DSPG (3:1) membrane.

The MD simulations presented so far involved a single AuNP. It is also relevant to consider cases with several AuNPs as they may reveal concentration-dependent phenomena. We used the CG model based on the Martini force field for studying the cooperative effect of several nanoparticles acting simultaneously on pure DSPC and DSPC/DSPG (3:1) bilayers. The results for the latter case are presented in **Figure 7**A, where we show the evolution of the lateral partial density of AuNPs and DSPG lipids over the simulation time. In the beginning, 16 AuNPs are placed on the membrane surface in an equidistant manner. During the subsequent MD simulation at 343 K, the system displays a rapid evolution toward nanoparticle aggregates on the membrane surface, as seen after 4 μs. The corresponding partial density analysis of DSPG lipids highlights a higher local concentration of the negative lipids in the vicinity of the AuNPs. Further investigation reveals that 25 mol% of DSPG lipids are located in between AuNPs forming thereby a negative counter-charge layer between the positively charged nanoparticles.

One example of AuNP aggregates is visualized in Figure 7B, where a trimer configuration is highlighted. Both DSPC and DSPG lipids crawl all over the nanoparticles, while they (especially DSPG) also bind the AuNPs together in a nearly-linear shape by screening and counterbalancing AuNP charges. The lipid extraction ("crawling") is evident even on individual AuNPs. The present aggregate is an excellent example of aggregate formation, and it demonstrates local perturbations in the lipid bilayer. Together with the previous observation for a

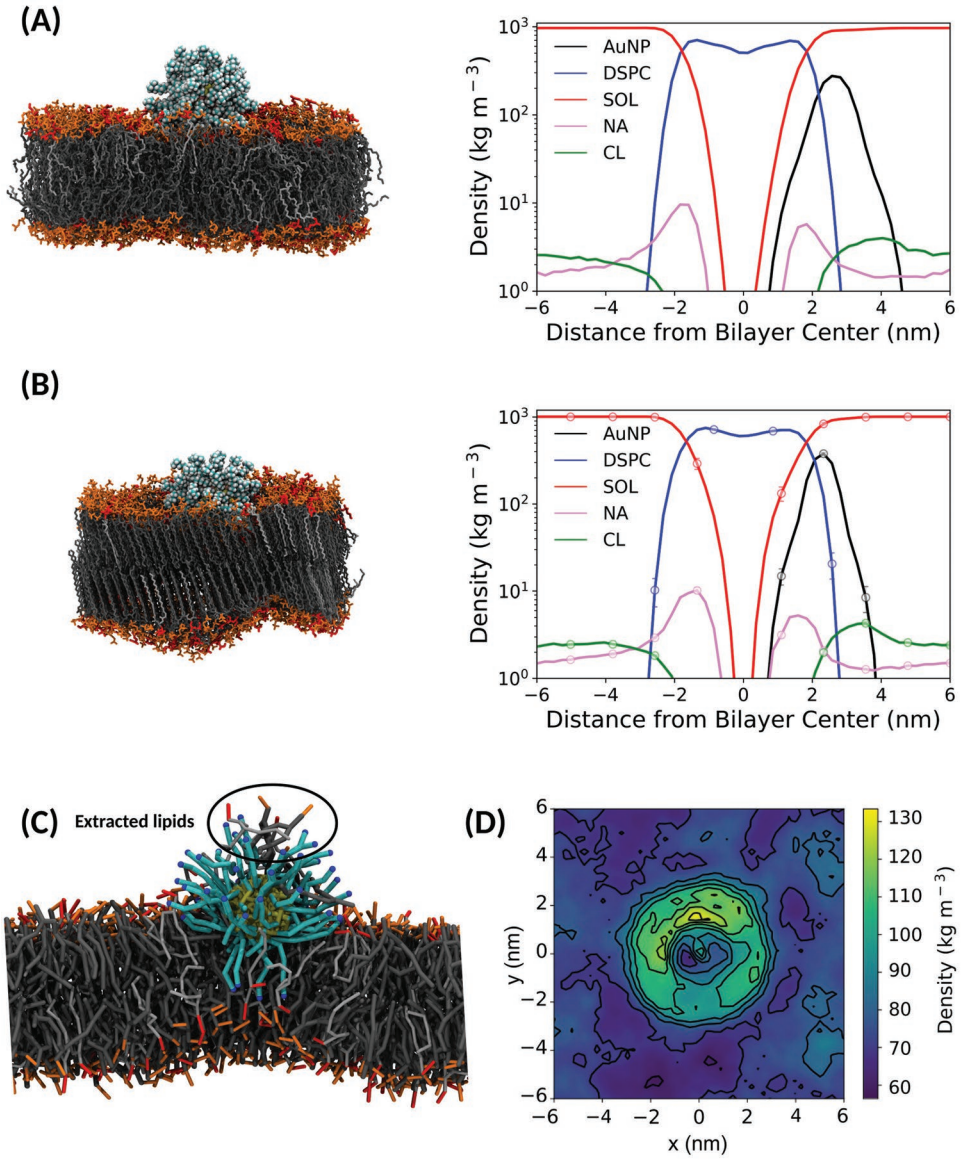


**Figure 6.** A) Left, a snapshot of AuNP interacting with the DSPC/DSPG (3:1) membrane surface taken from the AA simulation at 343 K after 200 ns. As in Figure 4, the lipids are visualized in licorice style where the color distinguishes between DSPC and DSPG. Right, the respective partial density profile averaged over the last 50 ns. B) Left, a snapshot of AuNP interacting with the DSPC/DSPG (3:1) membrane surface from the AA simulations taken after 200 ns of cooling down simulation to 300 K (gel phase). Right, the corresponding partial density profile averaged over the last 50 ns. The standard error is calculated considering the three repeated simulations as independent samples. C) A snapshot from the coarse-grained simulation at 343 K after 21 µs showing the lipid extraction effect for the DSPC/DSPG (3:1) membrane. The coarse-grained AuNP is in licorice style where the color code is the same with the exception of the AuNP core (yellow). D) Lateral concentration of DSPG lipids from the CG simulation of DSPC/DSPG (3:1) membrane at 343 K averaged over the last microsecond.

single AuNP in Figure 6B, this result indicates that the presence of AuNPs may reduce the stability of the DSPC–DSPG (3:1) bilayer by lipid extraction, which also involves the lower leaflet by inducing asymmetry in the number of lipids between the layers.

To compare with the result obtained for the pure DSPC layer, we present the pair-correlation function of AuNPs in Figure 7C for the DSPC and DSPC-DSPG (3:1) bilayers at 343 K. The contrast between the two cases is evident: While the aggregation is visible for DSPC–DSPG (3:1) as a finite weight at small distances, the pure DSPC layer does not exhibit oligomers (Figure S8, Supporting Information). This phenomenon confirms the critical role played by DSPG in promoting the aggregation behavior.

## 3. Discussion

We have presented experimental and in silico studies of the effect of cationic AuNPs on the structure of planar lipid bilayers with different amounts of charged lipids in two different phases (i.e., gel and liquid phases). Our approach

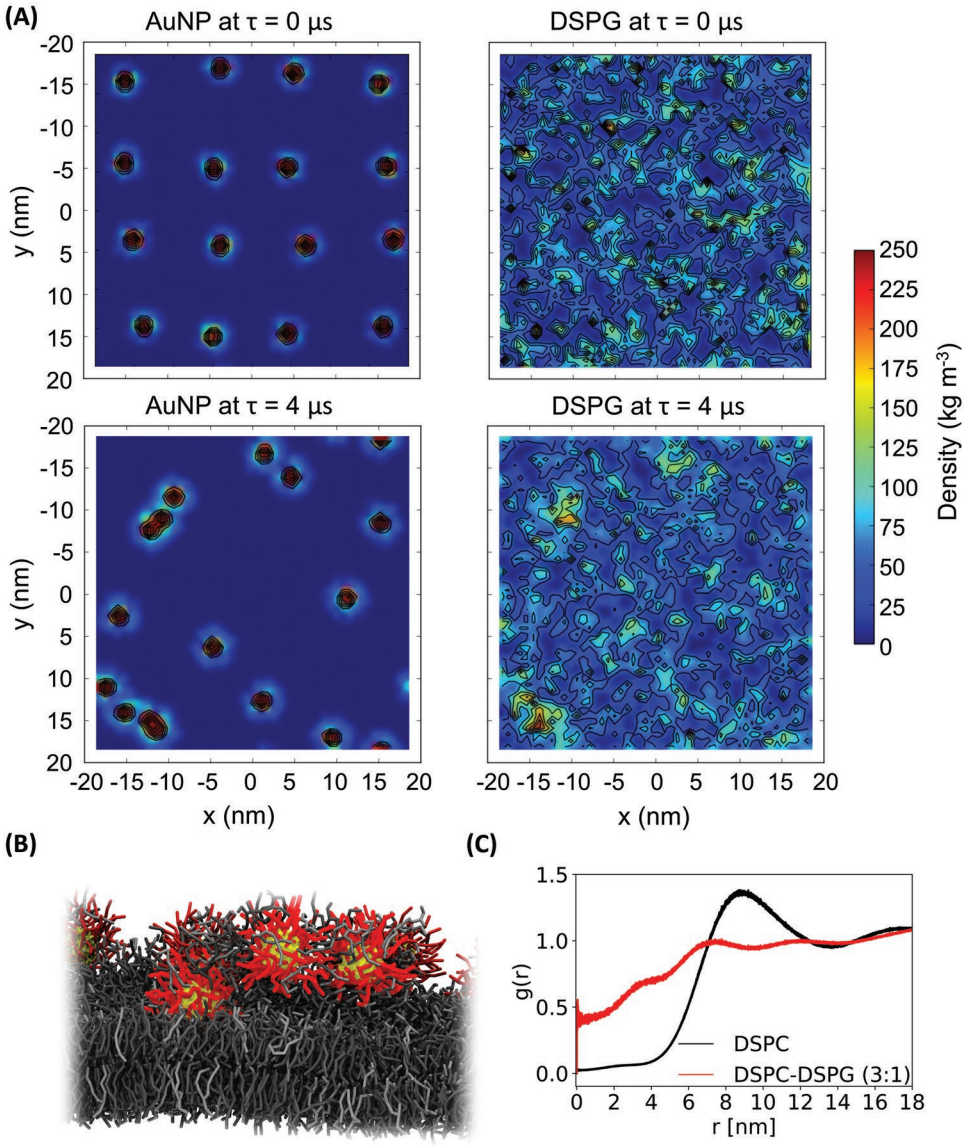


**Figure 7.** A) Lateral partial density analysis of AuNPs (left) and DSPG lipids (right) at $\tau \approx 0$ (top row) and a $\tau \approx 4\,\mu s$ (bottom row). The analysis is averaged over the first and last 50 ns, respectively, of the CG simulation with 16 AuNPs on the DSPC/DSPG (3:1) bilayer (4608 lipids) at 343 K. See Video S2 in the Supporting Information for the partial density analysis during the whole trajectory. B) Snapshot of AuNP trimer formation at 4 μs in the CG simulation. All molecules visualized in licorice style. The AuNP side chains are colored in red, the Au core is in yellow, and the bilayer is colored by using grey scale. The DSPC and DSPG lipids are dark and light gray, respectively. Water and counter-ions are removed for clarity. C) Averaged pair correlation functions of the AuNP–AuNP pairs during the last 1 μs of the CG simulations with 16 AuNPs on pure DSPC (black line) and DSPC/DSPG (3:1) (red line).

allowed us to quantify the effect of charged lipids on the interaction between AuNP and model lipid membranes using both experimental and theoretical methods, which together provided us with information at the molecular level. To characterize comparable systems, the MD simulations used AuNPs with sizes and compositions similar to those used in the experiments. Furthermore, the lipid membranes also had the same compositions. We acknowledge that there are differences between the two methodologies and particular care must therefore be taken when comparing the results. The primary difference regards the accessible time scales. While neutron reflectometry provides information about systems under equilibrium conditions at time scales of minutes or hours, MD simulations explore the system of interest over time scales of microseconds (AA models) or milliseconds (CG models). Further, lipid bilayers studied in our experiments floated above supported bilayers, while the simulations were carried out for freely standing bilayers. Given these differences, the two techniques give complementary and coherent views of the membrane systems, and the results provide detailed information on the effect of AuNPs.

For a pure DSPC lipid bilayer, the NR measurements gave experimental evidence for AuNP incorporation. This incorporation occurred only within the floating lipid bilayer and

did not involve the supported bilayer. The AuNP incorporation was accompanied by structural changes in the bilayers. Besides the structural change of SLD observed in the tail region of the floating bilayer due to the Au core, we observed that notwithstanding the value of coverage of the floating bilayer remained the same, the hydration of the membrane region declined. We interpreted this as incorporation of the AuNP inside the floating bilayer with consequent displacement of water molecules. This conclusion relies on the fact that the NR measurements were performed at different isotopic compositions of the aqueous phase, which enabled us to disentangle the SLD contribution of the solvent from those of the other components. Another effect resulting from the AuNP inclusion is a significant increase (≈70%) of the separation between the supported and floating bilayer. This effect was already seen for pure DSPC floating bilayer systems when approaching the gel to liquid transition temperature.[39,40] In the presence of cationic AuNP, this effect persists at room temperature. Interestingly, the incorporation of AuNPs was achieved only after the temperature had been increased to a value close to the gel to fluid phase transition of the lipid bilayer. This indicated that the interaction between the cationic AuNPs and DSPC lipid bilayer is modulated by a free energy barrier, which was confirmed by biased MD simulations (32 kJ $mol^{-1}$). Further MD simulations revealed that the transmembrane state of AuNP corresponds to a deep well of –200 kJ $mol^{-1}$. This is supported by the NR measurements that evidenced stable conditions for AuNPs inside the DSPC floating lipid bilayer, even after copious solvent flow through the experimental cell. According to MD, the AuNP translocation path inside the bilayer is associated with a circular patch opening in the bilayer surface upon adsorption as the cationic terminal groups (AuNP) and phosphate head groups (lipids) bend away from the contact area. While the number of ionic contacts between AuNP and DSPC does not change, this initial reorganization of lipids weakens interplanar interactions (ionic, hydrophobic) on the bilayer surface resulting in a small free energy cost (barrier).

The negatively charged DSPC/DSPG (3:1) bilayer showed remarkably different behavior in the presence of cationic AuNP. After injection and 30 min incubation of cationic AuNP in the aqueous solution, the reflectivity profile analysis showed a layer of AuNPs adsorbed on the floating lipid bilayer due to the attractive interaction between the positive terminal (choline) groups of AuNP and negatively charged lipid head groups. Unlike for pure DSPC, the nanoparticles were not incorporated into the floating bilayer in a stable manner, and annealing removed the adsorbed AuNP layer. Interestingly, the AuNP layer desorption was accompanied by lipid extraction, as evidenced by the reduced coverage (≈13% less) of the floating bilayer (Table S2, Supporting Information). The MD results for the DSPC/DSPG (3:1) lipid bilayer suggest a possible mechanism that could be responsible for the lipid extraction. The presence of AuNP causes a nonhomogeneous local distribution of DSPC/DSPG lipids, which can also crawl on the AuNP surface (see Figure 6C). Notably, the negatively charged DSPG can stick between the cationic nanoparticles effectively "glueing" them together to aggregates, while reducing the net charge and then the attractive interaction between AuNPs and the rest of the bilayer. The subsequent AuNP departure removes the attached/crawling lipids away from the bilayer.

The NR experiments performed at the intermediate DSPC-DSPG (9:1) composition neither showed a clear AuNP incorporation in the bilayer center, as for DSPC, nor a simple adsorption on the surface, as for DSPC-DSPG (3:1). The analysis pointed rather to a more disordered phase in the floating bilayer as we could not fit the data with the well-defined head–tail sequence structure typical for lipid bilayers. The data were interpreted by introducing a model that involves a partial incorporation (up to ≈20%) of AuNP inside the outer leaflet of the floating bilayer (see Figure 3). The onset of this partial AuNP incorporation was triggered by increasing the temperature up to 65 °C, again. MD simulations were not performed for the DSPC–DSPG (9:1) bilayer because the atomistic bilayer model (512 lipids) could not represent realistically the presence of only 10 mol% of DSPG lipids with AuNP; almost all DSPG lipids would become organized around the nanoparticle (charge of +46) in this case. Based on the collected results, we postulate the following explanation: The DSPG migration beside and over AuNP weakens the interaction with the membrane surface. There is more DSPG available for the 3:1 composition, which enable more AuNP to escape. In the case of DSPC–DSPG (9:1), AuNPs can still get incorporated within the membrane prior to the aggregate formation (effect observed for pure DSPC). This is also consistent with the initial adsorption within the gel phase observed for the (3:1) case.

MD simulations revealed also other important details which are not visible with NR. Concerning the bilayer structure, the presence of the cationic AuNP resulted in opposite changes in the curvature for the DSPC and DSPC/DSPG (3:1) lipid bilayers. This is caused by the detailed atomistic interaction between the lipid head groups and AuNP side chains, where interdigitization with DSPG pulls AuNP more tightly on the surface. We observed that the AuNP presence on one side of the bilayer affected not only the leaflet in question, but also the other leaflet on the opposite side. The effect is enhanced for DSPC/DSPG (3:1), and a longer CG simulation revealed that the membrane beneath AuNP became occasionally "punctured" as AuNP side chains extended ("snorkeled") toward the other side of the bilayer (Figure 6C). Despite the short time scales, some lipids could be seen to leave the bilayer and crawl over AuNP even in the AA simulations, and this became more evident with CG.

Of particular importance is the collective behavior of several AuNPs on laterally extended model membranes, which we modelled with CG simulations on a microsecond timescale. Our simulations confirmed the lipid crawling effect, but yet, something more significant occurred. We found a strong AuNP aggregation effect where the negative DSPGs act as a binding medium between the cationic nanoparticles. The AuNP aggregates induce a lipid concentration inhomogeneity, and together with lipid crawling and the effects on the lower leaflet this points to membrane instability for the DSPC–DSPG (3:1) system, fully inline with the experimental results. On the other hand, AuNP aggregation could not be observed for the pure DSPC bilayer, which behaved in a stable manner. The

negative charge of DSPG plays a crucial role here, as the origin of these phenomena lies mostly in the Coulomb interactions between lipid head groups and AuNP side chains.

## 4. Conclusions

We have studied cationic AuNPs interacting with floating lipid membranes composed of different mixtures of zwitterionic DSPC and negatively charged DSPG lipids. The interest of studying negatively charged membranes lies in the fact that plasma membranes contain negatively charged lipids, especially on the cytosolic side. Experimentally, while DSPC lipid bilayers showed a tendency to incorporate cationic AuNPs, negatively charged lipid bilayers composed by a 3:1 mixture of DSPC/DSPG lipids displayed surface adsorption of cationic AuNPs that led to membrane destabilization. Atomistic and coarse-grained MD simulation of symmetric lipid bilayers using the same AuNPs and membrane compositions validated the experimental conclusions and provided additional molecular insights. In particular, we report the pathway for AuNP insertion inside model membranes at higher temperatures (343 K) for zwitterionic DSPC bilayers, a mechanism for lipid extraction of adsorbed AuNP, and a potentially harmful AuNP aggregation effect for negative bilayers containing 25 mol% DSPG. According to our knowledge, the AuNP concentration effect (through several AuNPs) on membrane properties has received very little attention by MD simulations prior to our work.

## 5. Experimental Section

*Simulation Protocol*: *Atomistic Simulations*—All atomistic and coarse grained simulations were conducted by using GROMACS 5.1.4 simulation package.[45] The AuNP was first simulated in water at 300 K at physiological salt concentration (NaCl 0.15 M) for 300 ns. Two different DSPC:DSPG mixture lipid membrane compositions were prepared by using the Charmm-gui web server[46] and were equilibrated for 200 ns in the *NpT* ensemble. Afterward, the equilibrated nanoparticle was placed above the membrane surfaces with a minimum distance of 2 nm. This system was equilibrated in the *NpT* ensemble at 343 K for 100 ns by applying harmonic restrains to the nanoparticle on the *z*-axis. The same protocol was applied to both pure DSPC and DSPC/DSPG (3:1) systems. To study the possible insertion mechanism, the nanoparticle was placed at two other distances from the membrane center-of-mass: 4.6 nm (on the membrane surface) and 0 nm (inside the membrane); see Table S7 in the Supporting Information for the time table of the simulations. To reach the above described distances, the nanoparticle was gently pulled from the original configuration (6 nm far from the bilayer center) by applying a harmonic potential with a constant of 2000 kJ $mol^{-1}$ $nm^{-2}$ and a pull rate of $5 \times 10^{-3}$ nm $s^{-1}$. For the 25% DSPG membrane system, the frame where the nanoparticle spontaneously attached to the membrane surface (distance ≈4.5 nm) was used as the starting point. For all the other cases, the system was pre-equilibrated at that distance for 100 ns by using and harmonic restraint with a constant of 2000 kJ $mol^{-1}$ $nm^{-2}$.

All the systems were subjected to energy minimization using the steepest descent algorithm. After the minimization the systems were equilibrated in the *NpT* ensemble by using the Berendsen thermostat[47] with a time constant of 1.0 ps. The time step was set to 2 fs for the production run, and temperature was kept constant by using the V-rescale thermostat[48] with a time constant of 1 ps. A semi-isotropic constant pressure of 1 bar was employed by using the Parrinello–Rahman barostat[49,50] with a time constant of 5 ps. Electrostatics were handled with the PME algorithm of the order of 4.[51]

*Coarse Grained Simulations*: Two different simulations at 343 K with AuNP placed in the water phase, in presence of pure DSPC and DSPC–DSPG (3:1) membrane were performed to validate the MARTINI model by comparison with the AA simulations. After validating the CG model, two systems with 16 nanoparticles placed in the vicinity of a 4608 lipid membrane surface were built and simulated for both lipid membrane compositions. The models were constructed by using the same method employed in the atomistic section to mimic the nanoparticle membrane adsorption on the pure DSPC membrane. One system for each lipid membrane composition was simulated for 4 µs. The quantitative analysis was made on those samples see Table S7 in the Supporting Information for the time table of the simulations). The optimal time step for stable CG simulations was 14 fs, and the temperature was kept constant as before for the AA simulations by employing the V-rescale algorithm. Unlike for the AA simulations, the semi-isotropic condition were satisfied with the Berendsen barostat[47] to ensure a stable system over a long simulation time without any crashes.

Due to the high number of positive charges in AuNP (46+), the long range electrostatic interactions must be taken into account properly; they were treated with the PME method with an order of 4 and Fourier grid spacing of 0.12 $nm^{-1}$.

*Chemicals*: DSPC, DSPG and perdeuterated DSPC were obtained in powder form (chemical purity >99%) from Avanti Polar Lipids (Alabaster, AL) and dissolved without further purification in spectrograde chloroform (Sigma-Aldrich) to prepare solutions of $1 \times 10^{-3}$ M total lipid concentration. Distilled water was purified with a Milli-Q Gradient System (Millipore, Bedford, MA) to produce ultrapure water with a resistivity of 18.2 MΩ cm. Octanethiol ($C_8H_{18}SH$, 99%), hydrogen tetrachloroaurate(III) trihydrate ($HAu^{III}Cl_4 \cdot 3H_2O$, ⩾99.9%), sodium borohydrate ($NaBH_4$, 99%), and tetraoctyl-ammonium bromide [$(C_8H_{17})_4NBr$, 98%] were obtained from Sigma-Aldrich and used as received for the gold nanoparticle preparation.

*Gold Nanoparticles and Lipid Systems—Preparation of Cation-Functionalized Nanoparticles*: The AuNP were synthesized and characterized by following the same procedure described in reference.[6] Briefly, octanethiolate-capped AuNP ($C_8SAu$ NPs) were synthesized with the two-phase methods developed by Brust et al.[52,53] The functionalization with the cationic group was done via Murray place-displacement reaction[54] by stirring 150 mg of $C_8SAu$ NPs and 150 mg of *N*,*N*,*N*-trimethyl(11- mercaptoundecyl)ammonium chloride in 20 mL of degassed tetrahydrofuran under argon for two days at room temperature. The obtained cationic functionalized AuNPs ($Me_3N^+AuNPs$) had a radius around 2nm and a rate of exchange of the original octanethol capping for the ω-thiol trimethylammonium chloride ligand of around 70%.[6]

*Gold Nanoparticles and Lipid Systems—Preparation of Floating Lipid Bilayers*: Prior to the lipid deposition, highly polished silicon single 111 crystals ($8 \times 5 \times 1.5$ $cm^3$) were cleaned by sonication in chloroform and acetone, then exposed to a continuous flow of ozone for 30 min in order to render the substrate surface highly hydrophilic.

The first three layers of the lipid system were prepared with the Langmuir–Blodgett method with the following procedure: the lipid (or lipid mixture) was dissolved in chloroform and deposited drop-wise on the water surface of the Nima Technology LTD (Coventry, England) trough having a surface area of 600 $cm^2$ and computer controlled barriers and dipper. Surface pressure was measured via an electronic pressure sensor with precut paper Wilhemly plates (wet perimeter 20.6 mm; weight 80 mg $m^2$). The water in the trough was thermostated at 20 °C using a refrigerating/heating circulator (Fisher Scientific). The system was let equilibrate for 30 min and then compressed at a rate of 20 $cm^2$ $min^{-1}$ to a surface pressure of 40 ± 0.1 mN $m^{-1}$. The transfer ratios for these layers were 0.94 ± 0.5. The floating lipid bilayer was completed by a final horizontal Langmuir–Schaefer deposition of the same lipid composition as the three first layers to obtain symmetric zwitterionic or anionic bilayers. The samples and their lipid composition used in the experiments are listed in **Table 1**.

**Table 1.** Lipid composition of the floating lipid bilayers used in this study.

| | DSPC [% ] | DSPG [% ] | d-DSPG [% ] |
|---|---|---|---|
| Sample 1 | 100 | 0 | 0 |
| Sample 2 | 75 | 0 | 25 |
| Sample 3 | 90 | 10 | 0 |

As described elsewhere,[39] the samples were sealed with a polytetrafluoroethylene (PTFE) lid directly in ultrapure water and transferred to an aluminium cell thermostated with a water circulation bath (Haake) at the beam line with a feedback temperature obtained with a PT100 sensor. The PTFE lid was equipped with inlet and outlet holes to change the different subphases. Following the Langmuir–Blodgett/Langmuir–Schaefer depositions, all the pristine lipid bilayers were annealed above the gel–fluid phase transition temperature of the lipids. The annealing process was done both to remove possible structural defects occurring during the preparation and to confirm the stability of the floating bilayer in the fluid phase.

*Neutron Reflectometry*: In a neutron reflectivity experiment the ratio between the intensity of the incident and reflected neutron beam is measured as a function of the momentum transfer, $Q_z$ in the direction perpendicular to the interface.[55] The reflectivity as a function of $Q_z$ is related to the scattering length density profile, $\rho(z)$, along the direction perpendicular to the interface that can be defined as

$$\rho(z) = \sum_j b_j n_j \tag{1}$$

where $b_j$ and $n_j$ indicate the scattering length and the number of the nuclei $j$. The analysis of reflectometry data involves the description of the interface in terms of a series of parallel layers each characterized by an average scattering length density, thickness, and roughness. The parameters of this model are used to calculate the reflectivity profile.[56–58] The calculated profiles are then compared to the measured ones in a fitting procedure whose quality is assessed by using $\chi^2$.

Contrast variation is used to solve one of the common problems in neutron reflectometry, i.e., the absence of strict one-to-one relationship between the reflectivity profiles and the scattering length density profiles, i.e., more scattering length density profiles can theoretically be linked to a single reflectivity profile. To resolve this indetermination it is common practice to perform a series of measurements on the same system having different isotopic compositions. A typical series of measurements for example consist of performing the reflectometry with different deuteration level of the liquid subphase. It is assumed that the main nanostructural features do not change relevantly by substituting water and $D_2O$, but the reflectivities, and consequently the scattering length density profiles, change significantly. Simultaneous corefinement of reflectivity curves performed at different contrasts and a previous physical knowledge of the studied system help to extract a unique model of the interface.[59]

Reflectivity measurements were performed on the D17[60] reflectometer at the ILL, Grenoble (France) in the time-of-flight mode. The neutron beam wavelength $\lambda$ ranged between 2 and 25 Å with two incoming angles of 0.8° and 3.2°. The solid–liquid interface cell was oriented vertically and kept in position while changing solvents. Measurements were performed at the silicon/water interface with the beam transmitted through the silicon block. Different isotopic compositions of water were used: $D_2O$ (Contrast 1), a combination of $D_2O$, $H_2O$ giving a SLD of $4 \times 10^{-6}$ Å$^{-2}$ (Contrast 2) (4MW), one matching the SLD of silicon (Contrast 3) and $H_2O$ (Contrast 4). The SLD of the bulk phases were however fitted to account of possible incomplete exchange of the solvents.

Data were analyzed using Motofit[61] allowing simultaneous fitting of data sets from the same sample under different contrast conditions. Motofit models the interface by a series of parallel layers of homogeneous material each characterized by an averaged SLD, weighted on all of its nonwater components, a thickness and an interfacial roughness. The model reflectivity profiles are calculated using the Abele's method[56,57] with the error between two consecutive layers described by an error function.[58] The least-square optimization of the fitting parameter is done with Genetic optimization algorithm. The parameters uncertainties are obtained from their covariance matrix and their error correspond to a $\Delta\chi^2/\chi^2$ of 5%. In order to improve the description of the experimental data and account for not complete coverage of the floating bilayer, the model used was modified to take into account the possibility of having macroscopical regions where the floating bilayer was not present. If the interface is composed by regions with different SLD profiles $\rho_1(z)$ and $\rho_2(z)$ (e.g., region 1: a lipid bilayer floating above a supported bilayer; region 2 a supported bilayer only), the total reflectivity is a linear combination of the reflectivities of the two regions

$$R(Q_z) = x_1 R_1(Q_z) + (1 - x_1) R_2(Q_z) \tag{2}$$

where $R_1$ and $R_2$ are the reflectivities of the two domains and $x_1$ is the fraction of the illuminated area covered by the first domain. The fitting obtained with MotoFit will be referred as Fit Method I hereafter.

In lipid bilayers the roughness, $\sigma$, propagates between the heads and tail regions of different leaflets. In order to respect this physical feature, we made the choice to constrain $\sigma$ to a single value for each sublayer (head-tail-tail-head) within a lipid bilayer. Especially in the case of the thinner head layers, this can sometimes bring the value of the roughness close to that of its thickness. However, this choice reduces considerably the number of free parameters in the fit based on realistic physical assumption and accordingly it minimizes possible covariance between parameters.

In one case, the fitting results were further refined using an in-house developed algorithm that modeled the SLD profile based on the volume distribution of the different chemical species present at the interfaces (e.g. lipid heads, lipid tails, AuNP core, AuNP ligands). The volume fraction distributions of different molecular species was calculated as a function of the position across the interface, $z$, according to their relative position and were linked with some relevant functional constraints such as the number of lipid tails with respect to the number of lipid heads and the number of ligands per AuNP (see the Supporting Information).

A SLD profile obtained by the volume fraction distributions discretized in slices 1 Å thick, was used to calculate the reflectivity curves associated to this SLD profile. The calculated reflectivity profile was compared to the experimental by means of the $\chi^2$. Successively, another SLD profile was generated following a random change in one of the parameters that build it and a new reflectivity curve was obtained and compared with the experimental one. If the $\chi^2$ was reduced the change was accepted otherwise it was accepted following the Metropolis Monte Carlo criteria.[62] The uncertainties on the parameters were calculated using the bootstrap analysis as done by other softwares.[63] The algorithm allows fits at multiples contrasts and will be referred as Fit Method II hereafter.

## Supporting Information

Supporting Information is available from the Wiley Online Library or from the author.

## Acknowledgements

F.L. and L.J. contributed equally to this work. The authors thank the Institut Laue Langevin for the allocation of beam time (doi:105291/ILL-DATA.8-02-574 and doi:105291/ILL-DATA.9-13-411) and the Partnership for Soft Condensed Matter for the use of the laboratories.

The authors thank the European Research Council, the Academy of Finland and the Magnus Ehrnrooth foundation for the financial support, and the CSC – IT Center for Science (Espoo, Finland) for computational resources. H.M.-S. acknowledges support from the European Regional Development Fund OP RDE (project ChemBioDrug no. CZ.02.1.01/0.0/0.0/16_019/0000729). The authors thank Dr. Sabina Tatur for the preparation of the AuNP samples and Dr. Robert Barker for technical assistance during the reflectometry experiments. The open access fee was covered by FILL2030, a European Union project within the European Commission's Horizon 2020 Research and Innovation programme under grant agreement N°731096.

## Conflict of Interest

The authors declare no conflict of interest.

## Keywords

gold nanoparticles, lipid membranes, molecular dynamics simulations, nanotoxicity, neutron reflectometry

Received: November 29, 2018
Revised: March 13, 2019
Published online:

[1] A. Nel, T. Xia, L. Mädler, N. Li, *Science* **2006**, *311*, 622.
[2] N. Lewinski, V. Colvin, R. Drezek, *Small* **2008**, *4*, 26.
[3] B. D. Chithrani, A. A. Ghazani, W. C. W. Chan, *Nano Lett.* **2006**, *6*, 662.
[4] Y. Roiter, M. Ornatska, A. R. Rammohan, J. Balakrishnan, D. R. Heine, S. Minko, *Nano Lett.* **2008**, *8*, 941.
[5] R. R. Arvizo, O. R. Miranda, M. A. Thompson, C. M. Pabelick, R. Bhattacharya, J. D. Robertson, V. M. Rotello, Y. S. Prakash, P. Mukherjee, *Nano Lett.* **2010**, *10*, 2543.
[6] S. Tatur, M. Maccarini, R. Barker, A. Nelson, G. Fragneto, *Langmuir* **2013**, *29*, 6606.
[7] T. Hauck, A. Ghazani, W. Chan, *Small* **2008**, *4*, 153.
[8] N. Khlebtsov, L. Dykman, *Chem. Soc. Rev.* **2011**, *40*, 1647.
[9] G. Fragneto, T. Charitat, J. Daillant, *Eur. Biophys. J.* **2012**, *41*, 10, 863.
[10] H. Wacklin, *Curr. Opin. Colloid Interface Sci.* **2010**, *15*, 445.
[11] E. Rascol, J.-M. Devoisselle, J. Chopineau, *Nanoscale* **2016**, *8*, 4780.
[12] A. P. Alivisatos, *Science* **1996**, *271*, 933.
[13] P. D. Jadzinsky, G. Calero, C. J. Ackerson, D. A. Bushnell, R. D. Kornberg, *Science* **2007**, *318*, 430.
[14] M. Walter, J. Akola, O. Lopez-Acevedo, P. D. Jadzinsky, G. Calero, C. J. Ackerson, R. L. Whetten, H. Grönbeck, H. Häkkinen, *Proc. Natl. Acad. Sci. USA* **2008**, *105*, 9157.
[15] O. Lopez-Acevedo, K. A. Kacprzak, J. Akola, H. Häkkinen, *Nat. Chem.* **2010**, *2*, 329.
[16] M. Brust, C. Kiely, *Colloids Surf., A* **2002**, *202*, 175.
[17] A. Labande, D. Astruc, *Chem. Commun.* **2000**, 1007.
[18] S.-Y. Lin, S.-W. Liu, C.-M. Lin, C.-h. Chen, *Anal. Chem.* **2002**, *74*, 330.
[19] R. A. Reynolds, C. A. Mirkin, R. L. Letsinger, *J. Am. Chem. Soc.* **2000**, *122*, 3795.
[20] C. J. Ackerson, P. D. Jadzinsky, G. J. Jensen, R. D. Kornberg, *J. Am. Chem. Soc.* **2006**, *128*, 2635.
[21] V. Rojas-Cervellera, C. Rovira, J. Akola, *J. Phys. Chem. Lett.* **2015**, *6*, 3859.
[22] V. Rojas-Cervellera, L. Raich, J. Akola, C. Rovira, *Nanoscale* **2017**, *9*, 3121.
[23] M.-C. Daniel, D. Astruc, *Chem. Rev.* **2004**, *104*, 293.
[24] E. C. Dreaden, A. M. Alkilany, X. Huang, C. J. Murphy, M. A. El-Sayed, *Chem. Soc. Rev.* **2012**, *41*, 2740.
[25] E. Heikkilä, A. A. Gurtovenko, H. Martinez-Seara, H. Häkkinen, I. Vattulainen, J. Akola, *J. Phys. Chem. C* **2012**, *116*, 9805.
[26] E. Heikkilä, H. Martinez-Seara, A. A. Gurtovenko, M. Javanainen, H. Häkkinen, I. Vattulainen, J. Akola, *J. Phys. Chem. C* **2014**, *118*, 11131.
[27] R. C. Van Lehn, M. Ricci, P. H. J. Silva, P. Andreozzi, J. Reguera, K. Voïtchovsky, F. Stellacci, A. Alexander-Katz, *Nat. Commun.* **2014**, *5*, 4482.
[28] R. C. V. Lehn, A. Alexander-Katz, *Soft Matter* **2015**, *11*, 3165.
[29] J. Lin, A. Alexander-Katz, *ACS Nano* **2013**, *7*, 10799.
[30] R. C. V. Lehn, A. Alexander-Katz, *Soft Matter* **2013**, *10*, 648.
[31] R. C. Van Lehn, A. Alexander-Katz, *J. Phys. Chem. A118*, 5848.
[32] P. Gkeka, L. Sarkisov, P. Angelikopoulos, *J. Phys. Chem. Lett.* **2013**, *4*, 1907.
[33] F. Simonelli, D. Bochicchio, R. Ferrando, G. Rossi, *J. Phys. Chem. Lett.* **2015**, *6*, 3175.
[34] G. Rossi, L. Monticelli, *Adv. Phys. X* **2016**, *1*, 276.
[35] X. Chen, D. P. Tieleman, Q. Liang, *Nanoscale* **2018**, *10*, 2481.
[36] A. Torchi, F. Simonelli, R. Ferrando, G. Rossi, *ACS Nano* **2017**, *11*, 12553.
[37] D. D. Silvio, M. Maccarini, R. Parker, A. Mackie, G. Fragneto, F. B. Bombelli, *J. Colloid Interface Sci.* **2017**, *504*, 741.
[38] A. Luchini, Y. Gerelli, G. Fragneto, T. Nylander, G. K. Palsson, M.-S. Appavou, L. Paduano, *Colloids Surf. B* **2017**, *151*, 76.
[39] T. Charitat, E. Bellet-Amalric, G. Fragneto, F. Graner, *Eur. Phys. J. B* **1999**, *8*, 583.
[40] G. Fragneto, T. Charitat, E. Bellet-Amalric, R. Cubitt, F. Graner, *Langmuir* **2003**, *19*, 7695.
[41] G. M. Torrie, J. P. Valleau, *J. Comput. Phys.* **1977**, *23*, 187.
[42] R. C. Van Lehn, M. Ricci, P. H. Silva, P. Andreozzi, J. Reguera, K. Voïtchovsky, F. Stellacci, A. Alexander-Katz, *Nat. Commun.* **2014**, *5*, 4482.
[43] S. Salassi, F. Simonelli, D. Bochicchio, R. Ferrando, G. Rossi, *J. Phys. Chem. C* **2017**, *121*, 10927.
[44] R. C. Van Lehn, A. Alexander-Katz, *PLoS One* **2019**, *14*, e0209492.
[45] M. J. Abraham, T. Murtola, R. Schulz, S. Páll, J. C. Smith, B. Hess, E. Lindahl, *SoftwareX* **2015**, *1–2*, 19.
[46] S. Jo, T. Kim, V. G. Iyer, W. Im, *J. Comput. Chem.* **2008**, *29*, 1859.
[47] H. J. C. Berendsen, J. P. M. Postma, W. F. van Gunsteren, A. DiNola, J. R. Haak, *J. Chem. Phys.* **1984**, *81*, 3684.
[48] G. Bussi, D. Donadio, M. Parrinello, *J. Chem. Phys.* **2007**, *126*, 14101.
[49] S. Nosé, M. L. Klein, *Mol. Phys.* **1983**, *50*, 1055.
[50] M. Parrinello, A. Rahman, *J. Appl. Phys.* **1981**, *52*, 7182.
[51] T. Darden, D. York, L. Pedersen, *J. Chem. Phys.* **1993**, *98*, 10089.
[52] M. Brust, M. Walker, D. Bethell, D. J. Schiffrin, R. Whyman, *J. Chem. Soc., Chem. Commun.* **1994**, *7*, 801.
[53] S. Tatur, A. Badia, *Langmuir* **2012**, *28*, 628.
[54] M. J. Hostetler, S. J. Green, J. J. Stokes, R. W. Murray, *J. Am. Chem. Soc.* **1996**, *118*, 4212.
[55] J. Penfold, R. K. Thomas, *J. Phys.: Condens. Matter* **1990**, *2*, 1369.
[56] O. S. Heavens, *Optical Properties of Thin Films*, Butterworth, London **1955**.
[57] F. Abelès, *J. Phys. Radium* **1950**, *11*, 307.
[58] L. Nevot, P. Croce, *Rev. Phys. Appl.* **1980**, *15*, 761.
[59] T. Crowley, E. Lee, E. Simister, R. Thomas, *Physica B* **1991**, *173*, 143.
[60] R. Cubitt, G. Fragneto, *Appl. Phys. A* **2002**, *74*, s329.
[61] A. Nelson, *J. Appl. Crystallogr.* **2006**, *39*, 273.
[62] N. Metropolis, S. Ulam, *J. Am. Stat. Assoc.* **1949**, *44*, 335.
[63] Y. Gerelli, *J. Appl. Crystallogr.* **2016**, *49*, 330.